University of Bristol

DEPARTMENT OF COMPUTER SCIENCE

Ultrasound Speckle Tracking For Strain Estimation

J. Revell, M. Mirmehdi and D. McNally

December 2003 | CSTR-04-005

Ultrasound Speckle Tracking For Strain Estimation

J. Revell and M. Mirmehdi
University of Bristol
Department of Computer Science
{revell, majid}@cs.bris.ac.uk

D. McNally
University of Nottingham
Institute of Biomechanics
Donal.Mcnally@nottingham.ac.uk

Abstract

This paper presents an alternative to Elastography by speckle tracking ultrasonic frames quantifying both motion and strain. We combine two similarity measures for varying echographic content including displacement processing, with interframe and trajectory performance measured on extensive synthetic and in vitro data.

1. Introduction

With modern ultrasound machines providing realtime sequence digitisation, motion estimation research in this area for noise filtering, tracking and registration has increased. In this paper we investigate a novel practical alternative to elastography using speckle tracking to infer tissue motion and to estimate strain. We focus on extensive synthetic and *in vitro* sequence interframe and trajectory displacement accuracy determining strain precision. Our contribution includes using two speckle pattern similarity measures, adapting to regions of varying signal and noise using a multiresolution approach with velocity vector post-processing.

Elastograms quantify strain from an applied stress using ultrasound [8], displaying the longitudinal strain as the axial component of the estimated displacement gradient. Displacements are derived from 1D cross correlation of radio frequency (RF) echo arrival times pre- and post-compression. Elastography drawbacks include the inability to record and store RF data restricting clinical usability and typically limited to measuring small strains of only $<1\%$.

Speckle tracking can provide real solutions to many of these problems, with existing research including Meunier and Bertrand [6] and Bohs et al. [3], all noting its importance to model tissue behaviour. More recently Cohen and Dinstein [5] and Boukerroui et al. [4] use an alternative speckle matching measure (CD_2), that assumes the speckle patterns in ultrasound images can be represented by a multiplicative Rayleigh distributed noise.

In our recent work [7] accurate interframe displacements and motion trajectories of individually tracked blocks were achieved, using hierarchical blocks and a multiple scale normalised cross correlation (NCC) similarity measure. Focusing on musculoskeletal ultrasound, in deeper body regions a general reduction in correlation as a result of increased speckle noise was observed, affecting the correlation measure. Here, by combining multiple matching measures, we aim to maintain accuracy in strong signal regions using NCC as the first measure, with correlation reduction indicating necessary re-tracking using the alternative second measure CD_2.

In the next section we review speckle, filtering effects and the incorporation of the two matching measures. Section 3 details simulated and *in vitro* datasets with Section 4 defining vector post-processing, the strain tensor and error measurement. Section 5 shows our interframe, trajectory and strain results, finishing with a discussion in Section 6.

2. Speckle Pattern Similarity Measures

Tendons have a very striated structure, although no medium in the body is completely homogenous or flat. Scatter occurs when small imperfections (scatterers) cause seemingly random reflections and refractions of the sound wave. Scatterers account for a decrease in image quality, causing blurring and decreased intensity at impedance boundaries, while within the medium they create speckle. The statistics of the signal depends on the density of scatterers, with a large number of randomly located scatterers following a Rayleigh distribution (fully developed speckle). These conditions are seldom met, resulting in several different statistical models of speckle being used.

Much research has been aimed at removing speckle to enhance ultrasound image understanding, with many schemes producing reasonably homogenous regions, however, features that are the same scale as the speckle tend to be eliminated [9] impeding local motion estimation. Filter performance tends to be measured by quantifying edges and boundaries, with speckle preservation and fluctuation reduction measured using the co-occurrence matrix and lo-

calised mean and standard deviation. In our situation filtering is not applied, maintaining all echo information, consequently justifying a region-based motion estimation approach, which has some inherent robustness to speckle incoherence and machine noise for speckle tracking.

Although substantial research exists on analysing B-modes using low frequencies at $3-7$MHz (abdominal [5], cardiac and breast [4]), we focus on higher frequencies of mainly $8-16$MHz for musculoskeletal diagnosis, capturing higher resolution images at a reduced penetration depth. This is due to attenuation where the signal is reduced by approximately 1dB/cm/MHz.

Using three different probes with bandwidths $5-10$, $8-16$ and $10-22$MHz, we captured 30-frame sequences, using "perfect" conditions of an *in vitro* tendon section in a still water bath with clamped probe, and "less than perfect" conditions of an *in vivo* freehand scanning of the biceps. For all cases the images were spatially and temporally stable resulting in high tracking accuracy using our NCC tracking scheme. However the *in vivo* cases highlighted correlation reduction in areas corrupted by fully developed speckle that tend to occur in the lower regions, as illustrated in Fig. 1.

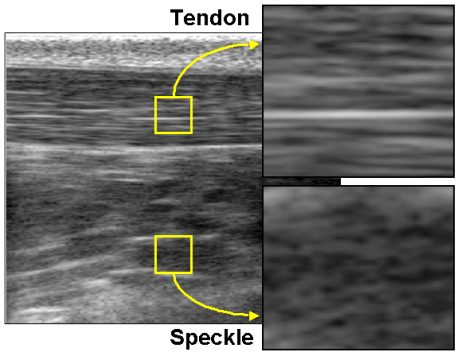

Figure 1. Achilles tendon with subimages of tendon and lower region speckle.

The first measure NCC, defined in [7], assumes an increased SNR from high frequencies and sparse scatterers as shown in the tendon region in Fig. 1. Although we have found the correlation typically high, as described above speckle noise reduces matching, highlighting the necessity of a suitable second measure. It must also be stated that other causes of correlation reduction are a lack of signal (probe de-coupling or curvilinear tendons), or signal saturation (incorrect gain controls or bone), or minimal features, causing problems for any similarity measure.

The second measure CD_2 introduced in [5] measures the error between two noisy blocks in an ultrasound sequence denoted $E_i^{CD_2}$. CD_2 assumes (to be matched) blocks x and y from f_t and f_{t+1} are corrupted by independent multiplicative Raleigh distributed noise, representing fully developed speckle. Log-compression transforms the multiplicative noise to additive obtaining a model for displayed ultrasound images, denoted as $\ln(x) = \tilde{x}$ and $ln(y) = \tilde{y}$. From [5] we maximise the CD_2 objective function [4] defined as:

$$E_i^{CD_2}(\mathbf{v}_i) = \sum_{j=1}^{N} \{(\tilde{x}_{i,j} - \tilde{y}_{i,j}) - \ln(\exp(2(\tilde{x}_{i,j} - \tilde{y}_{i,j})) + 1)\} \tag{1}$$

where i and j are the block and pixel index respectively.

Our proposed approach combines both measures using multiple scales with the NCC as the primary matching measure due to its high accuracy in the tendon region. The corresponding correlation coefficient is compared to a threshold value, set to 0.9 resulting from previous work and [6], establishing whether the same block should be re-tracked using the CD_2 secondary measure. The threshold value is sufficiently high to yield a good usage of the NCC and CD_2 measures in appropriate regions of varying scatterers. The CD_2 secondary measure is evaluated using the associated reference and candidate blocks in a full search with the same extents as the NCC primary measure. Results use block scales $M \times N = \{32, 16, 8\}$ sampling at 8×8.

3. Simulated and *In vitro* datasets

Simulated and *in vitro* data are used to compare known and measured displacements from the proposed method illustrating interframe and trajectory accuracy.

We implemented the commonly used method outlined in [6] simulating an echographic speckle sequence $I(x, y, t)$ where x, y and t denote the axial, lateral and temporal co-ordinates. The point spread function (PSF) $H(x, y)$ is assumed to be a Gabor function and the scattering function $T(x, y)$ a normally distributed random field that represents the population of scatterers being imaged. Convolving with the PSF yields the resulting RF echo data $I(x, y) = H(x, y) \otimes T(x, y)$, with envelope detection producing the desired image of echo magnitude. To measure robustness against noise we corrupted $I(x, y)$ with multiplicative Rayleigh noise η_m resembling speckle noise,

$$\hat{I}(x, y) = I(x, y)\, \eta_m \tag{2}$$

where $\eta_m \sim R(I) = \frac{I}{\sigma^2} \exp^{-\left(I^2/2\sigma^2\right)}$ with a non-zero mean specified by the single distribution parameter σ.

Using a Gaussian mask we simulated a central denser speckle region to provide boundary analysis. By applying known linear geometrical transforms including translation, rotation and affine deformation fields, various motions and corresponding strains can be analysed. Fig. 2 illustrates $I(x, y)$ with the corresponding displacement field, producing an equal decremental stiff background speckle and a uniformly high stiff central dense speckle.

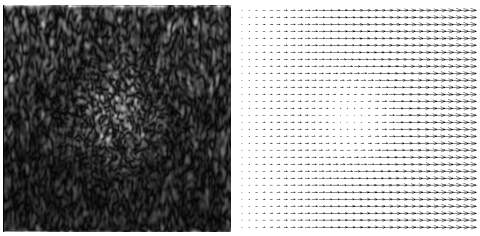

Figure 2. Simulated image and displacement field matching known geometric transform.

Several *in vitro* sequences were also captured using an equine tendon that was pulled 3, 6 and 10mm at known rates and loads whilst continuously scanning using an $8-16$MHz clamped probe. All sequences consist of 30 frames (the maximum acquisition length from the employed Diasus Dynamic Imaging ultrasound machine) captured at 30Hz and quantized into 8 bits. All cycles included a positive and negative pull, similar to *in vivo* extension to flexion motions.

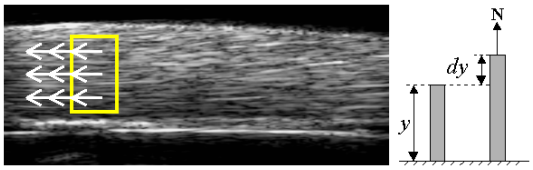

Figure 3. *In vitro* **groundtruth and setup.**

4. Displacement Processing, Strain and Error

Once the combined matching method is applied to our datasets we perform displacement processing. Spurious velocity vectors are inevitable from any tracking process and are not always obvious. Potential causes are from noise or artefacts where multiple block scales have insufficient encapsulated features. Using a coherence based post-processing algorithm, adaptive weighted vector median filter (WVMF) [1], displacements are smoothed if inconsistent with the dominant neighbours whilst preserving motion boundaries. Given the set V of N displacement vectors $\mathbf{v}_i = (v_x, v_y)$ the WVMF minimises the cumulative weighted p-norm distance from other vectors in V within a neighbourhood, defined as:

$$\sum_{i=1}^{N} w_i \|\mathbf{v}_m - \mathbf{v}_i\|_p \leq \sum_{i=1}^{N} w_i \|\mathbf{v}_j - \mathbf{v}_i\|_p \qquad (3)$$

where $\mathbf{v}_m$ is the local neighbourhood median vector, i and j are the individual centre and neighbouring vectors respectively and w the set of weights. Our adaptive weighting uses the NCC correlation coefficients ranging between 0 and 1. This technique lends itself to both interframe and trajectory smoothing whilst having low computation.

We also compute the 2D Lagrangian strain tensor ε from the displacement fields generating elastograms, defined as:

$$\begin{bmatrix} \varepsilon_x & \varepsilon_{xy} \\ \varepsilon_{yx} & \varepsilon_y \end{bmatrix} \text{ with } \begin{cases} \varepsilon_x = \frac{\delta x}{x} & \varepsilon_{xy} = \frac{\delta x}{y} \\ \varepsilon_{yx} = \frac{\delta y}{x} & \varepsilon_y = \frac{\delta y}{y} \end{cases} \qquad (4)$$

where ε_x and ε_y are the two normal directional strains and ε_{xy} and ε_{yx} are the two shear strains.

To quantify displacement accuracy the error between the known correct groundtruth velocity and the estimated velocity is measured by the angular error [2], that combines errors in magnitude and direction into a single value.

5. Simulated and *in vitro* Displacement Accuracy and Elastograms

Table 1 quantifies simulated interframe displacement accuracy with and without WVMF displacement processing. Cases included translation, rotation and affine warps of 1 and 5 pixels, 3° and 6°, and 2% and 4% respectively, with worst cases being corrupted by noise for a direct comparison. Cases postfixed with * denote displacement results

Table 1. NCC/NCC-CD$_2$ interframe accuracy.

	Noise	Angular Error		WVMF Angular Error	
Case	σ	Mean (°)	STD Dev (°)	Mean (°)	STD Dev (°)
1	—	0.00	0.00	0.00	0.00
1	0.8	2.87	8.77	1.21	2.24
1*	0.8	2.18	7.93	1.13	2.30
5	—	1.55	2.13	0.77	0.90
5	0.8	3.76	9.30	1.46	2.92
5*	0.8	2.94	10.32	1.28	2.27
3°	—	1.66	7.44	1.64	7.39
3°	0.8	2.90	9.90	2.00	7.62
3°*	0.8	2.28	8.87	1.95	7.09
6°	—	1.67	8.19	1.40	6.82
6°	0.8	3.47	11.33	2.41	9.26
6°*	0.8	3.27	10.12	3.20	9.38
2%	—	0.46	2.67	0.04	0.83
2%	0.8	3.88	13.21	1.90	7.74
2%*	0.8	0.58	2.97	0.07	1.05
4%	—	3.55	19.05	1.46	13.55
4%	0.8	5.58	20.47	2.77	13.26
4%*	0.8	2.74	16.07	1.03	8.98

from combining both NCC and CD$_2$ measures adaptively. These results illustrate a marked improvement compared to using the single NCC measure for the worst cases, due to a substantial increase in error and reduction in the correlation that ranged between $96.84\% - 99.99\%$ to $72.75\% - 78.15\%$ between best (— *no applied noise*) and worst $\sigma = 0.8$ cases. Using the WVMF showed noticeable improvements from just 1 iteration using an 8 neighbourhood region, and

showed no smoothing of the central denser speckle boundary. With more iterations obvious dominant regions of motion were visible. More results can be found online[1].

Fig. 4-left illustrates the required tensile load (N) to deform each specimen in our *in vitro* datasets by 3, 6 and 10 mm. Fig. 4-right shows a direct comparison of the corresponding groundtruth data to the measured trajectories. Each measured set of trajectories (region of individual block temporal displacements) quantifies the corresponding mean displacement (scaled to convert pixels to mm) for a tracked region using NCC-CD_2 combined measures and WVMF.

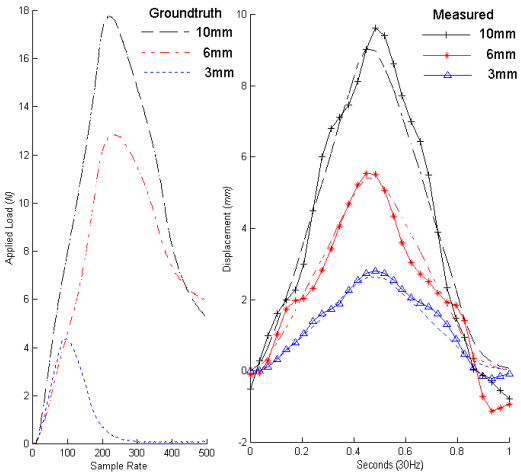

Figure 4. *In vitro* **trajectory displacements.**

Table 2 summarises the error between groundtruth and measured real displacements for the three *in vitro* experiments. The maximum error (MAX) is noticeable from Fig. 4 at the end of each pull cycle, when the tendon is not under load, that is due to the tendon not returning to its original resting state. Using a bone and achilles tendon interface reduced clamp slippage error and resulted in a relatively low mean absolute difference (MAD) for each sequence.

Table 2. *In vitro* **trajectory summary**

Pull (mm)	MAX	MAD	STD Dev
3	0.41	0.14	0.11
6	1.27	0.39	0.35
10	0.90	0.52	0.28

Sample elastograms are shown in Fig. 5 for our synthetic and *in vitro* data respectively. The synthetic elastogram shows the background tissue and central region strongly matching the applied deformation shown in Fig. 2, for the best case. The *in vitro* elastogram quantifies an increasing small strain in the direction of the pull (from left to right).

[1]http://www.cs.bris.ac.uk/~revell

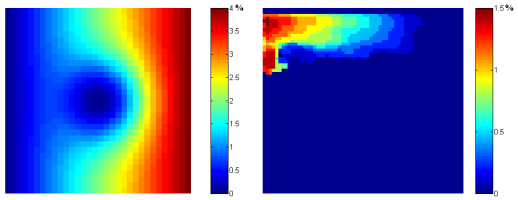

Figure 5. Synthetic and *in vitro* **data longitudinal elastograms ε_x.**

6. Discussion

We have demonstrated that using a combination of speckle pattern similarity measures improved interframe and trajectory performance validating our approach on synthetic data and *in vitro* datasets. Also by using WVMF, displacements have improved, reducing motion and strain error, weighted by the correlation confidence. WVMF showed accurate smoothing and support for motion boundaries, for example around the central stiff region in the simulated sequence. Using multiple similarity measures any displacement inaccuracy tended to be from motion induced noise, with normal solutions involving increased temporal sampling depending on tissue deformation rate.

The NCC consistently produced high correlation in the focused tendon regions, but reduced in the lower regions instigating the usage of the CD_2 measure. We observed that speckle tracking for strain estimation using ultrasound sequences has limitations, with large interframe tissue deformation $>15\%$ being increasingly difficult. Results indicate a strong advantage for using multiple similarity measures especially for obtaining reliable strain measurements with future work showing more strain tensor component results.

References

[1] L. Alparone, M. Barni, F. Bartolini, and V. Cappellini. Adaptively weighted vector-median filters for motion-fields smoothing. *ICASSP*, pages 2267–2270, 1996.

[2] J. Barron, D. Fleet, and S. Beauchemin. Performance of optical flow techniques. *IJCCV*, 12(1):43–77, 1994.

[3] L. Bohs, B. Friemel, and G. Trahey. Experimental velocity profiles and volumetric flow via two-dimensional speckle tracking. *UMB*, 21(7):885–898, 1995.

[4] D. Boukerroui, A. Noble, and M. Brady. Velocity estimation in ultrasound images: A block matching approach. *IPMI*, 2003.

[5] B. Cohen and I. Dinstein. New maximum likelihood motion estimation schemes for noisy ultrasound images. *ICPR*, 35:455–463, 2002.

[6] J. Meunier and M. Bertrand. Ultrasonic texture motion analysis theory and simulation. *TMI*, 14(2):293–300, 1995.

[7] J. Revell, M. Mirmehdi, and D. McNally. Strain quantification in ultrasound sequences. *BMVC*, 14:359–368, 2003.

[8] T. Varghese, E. Konofagou, J. Ophir, K. Alam, and M. Bilgen. Direct strain estimation in elastography using spectral cross-correlation. *UMB*, 26(9):1525–1537, 2000.

[9] Y. Yu and S. Acton. Speckle reducing anisotropic diffusion. *IEEE Trans. IP*, 11(11):1260–1270, 2002.